applied sciences

MDPI

Article

Outdoor Performance Comparison of Bifacial and Monofacial Photovoltaic Modules in Temperate Climate and Industrial-like Rooftops

Alejandro González-Moreno, Domenico Mazzeo, Alberto Dolara, Emanuele Ogliari * and Sonia Leva

Department of Energy, Politecnico di Milano, Via Giuseppe La Masa, 34, 20156 Milano, Italy; alejandro1.gonzalez@polimi.it (A.G.-M.); domenico.mazzeo@polimi.it (D.M.); alberto.dolara@polimi.it (A.D.); sonia.leva@polimi.it (S.L.)

* Correspondence: emanuelegiovanni.ogliari@polimi.it

Abstract: To fully exploit the advantages of bifacial PV (bPV) modules and understand their performance under real-world conditions, a comprehensive investigation was conducted. It was focused on bPV installations with some mounting constraints, as in industrial rooftops, where the ideal high module-to-ground height for optimal bPV performances is not feasible due to structural reasons. The experimental setup involved measuring the *I-V* curves of conventional and bifacial modules under diverse atmospheric conditions, including different solar irradiance levels and ambient temperatures, as well as mounting configurations. The results show a proportional increment of power generation between 4.3% and 7.8% if compared with two different conventional modules and a bifacial power gain between 2 and 15% under identical conditions. Additionally, the negative potential influence of the mounting structure was observed. Small differences in the alignment between the module and structural beams can virtually eliminate the bifacial contribution, with an estimated reduction up to 8.5 W (a potential bifacial gain of 3.43%).

Keywords: bifacial photovoltaics (bPV); bifacial performance; outdoor performance; *I-V* curve; industrial rooftop

Citation: González-Moreno, A.; Mazzeo, D.; Dolara, A.; Ogliari, E.; Leva, S. Outdoor Performance Comparison of Bifacial and Monofacial Photovoltaic Modules in Temperate Climate and Industrial-like Rooftops. *Appl. Sci.* **2024**, *14*, 5714. https://doi.org/10.3390/app14135714

Academic Editors: Manuela Sechilariu and Alejandro Pérez-Rodríguez

Received: 15 April 2024
Revised: 14 June 2024
Accepted: 25 June 2024
Published: 29 June 2024

1. Introduction

In the context of increasingly global energy demands and the vital importance of sustainable renewable energy sources, photovoltaic (PV) technology continues to play a pivotal role in meeting these challenges. Bifacial photovoltaic (bPV) technology has emerged as a promising solution, capable of converting sunlight from both the front and rear sides, potentially enhancing energy conversion efficiency compared to traditional PV modules. Two facts illustrate the relevance of bPV technology: the development of a specific IEC Standard to characterize bifacial devices (IEC 60904-1-2:2019 [1]) and the fact that Task 13 of the International Energy Agency (IEA) Photovoltaic Power Systems Programme (IEA PVPS) published a detailed report on bPV in recent years [2].

Production gains in the range of 6–10% under normal conditions have been reported [3–5], but considerable increments can be obtained with a proper design (+15–30%) and can be as high as 40% with optimal design parameters [6]. In order to take advantage of this potentiality, a thorough understanding of bPV technology is crucial, especially as a significant increment in worldwide bPV installation is expected. By 2030, the installation rate increased to 30%, while it was about 12% in 2020 [2].

Bifacial technology presents a promising avenue for sustainable land use and renewable energy generation. This innovative approach combines the benefits of both systems, leveraging the dual-sided energy capture capability of bPV modules and the land productivity enhancements offered by agrivoltaics. By deploying bifacial PV panels above agricultural fields, agrivoltaic systems can harness sunlight from both the front and rear

sides of the panels while simultaneously providing shade to crops or livestock below. This dual-use configuration increases the energy generation potential while optimizing land use efficiency [7]. Additionally, the presence of vegetation beneath the solar panels can enhance the performance of bifacial modules by increasing the amount of reflected and diffused sunlight reaching the rear side of the panels [8]. On the other hand, from an urban perspective, bifacial technology has a high potential of being integrated into energy-sustainable buildings [9]. Bifacial modules can be used as transparent or opaque façades, skylights, sunshades, and curtains or integrated into rooftops [9]. However, despite its architectural features, the energy production contribution of the bifacial modules requires a thorough analysis, paying special attention to the particularities of each installation.

Different parameters have been detected as crucial contributors to bPV performance. The main contributor is ground albedo (the percentage of incident sunlight that a surface reflects), as it proportionally increases the incident rear-side irradiance and, as a consequence, the rear power contribution. Daily albedo experiments [10,11] and seasonal variations [11] can be as high as 0.9 (fresh snow) [12,13] or as low as 5% (gravel) [11]. Another influential design parameter is the panel ground clearance height (GCH), which is the closest distance between the module and the ground. It has been found that its positive effect tends to saturate in the range of 0.4–1 m, depending on the location [14,15].

Module orientation (tilt and azimuth) can also have a positive effect, but the optimum is highly dependent on each specific site and may not coincide with the optimum for conventional modules [6,16]. Additionally, it has been highlighted that bifacial contribution increases when the diffuse to global radiation ratio is high [10], i.e., in overcast conditions.

As a counterpart, the bifacial contribution is reduced by the non-uniformity of the rear-side irradiance. Since the performance of any PV cell string is heavily influenced by the worst cell in the string, the increase in said non-uniformity, at the parity of the average component, would reduce the performance of the worst cell, diminishing the overall operation. Standard deviations of 30% of backlighting may occur with low mounted modules [14]. However, the effect can be reduced (ranging 2.8–4.1%) by increasing GCH [14], which links the positive effect of increasing GCH to its intrinsic reduction in back non-uniformity.

In particular scenarios, not all the optimal system parameters can be achieved. This is the case of industrial-like rooftops, where roof structural resistance limits module height, as it would increase both dynamic and static loads (wind-pressure loads and PV weight structure, respectively), intrinsically augmenting the rear non-uniformity. This can produce a considerable reduction in bifacial contribution due to the self-shading factor being considerably high (12.3–20%), even in specially designed structures [17]. The supporting elements (frames, beams, purlins, and piles) can obstruct backside irradiance about 20% in fixed tilted installations [18].

As a possible countermeasure, cold roofs with high albedo have been proposed [19]. As high albedo implies less radian energy translated into a local increment of ambient temperature, bPV modules will operate at lower local temperatures and higher back illumination. An albedo increment of 0.1 would imply an addition of 4.5% of energy production [19]. A recent research has tested a nanomaterial with extremely high albedo and thermal emittance (96% and 80%, respectively), which would imply an additional cooling of 20 W/m^2 (compared to sand) and an additional cell photocurrent of up to 6.42 mA/cm^2 [20].

Nevertheless, a notable increase in albedo could not necessarily imply a significant increase in production since non-uniform illumination induced by mounting structure can considerably reduce bifacial contribution [21]. From a potential bifacial power gain (BPG) of up to 23% at high albedo, it could be reduced to 5% just for the unevenness introduced by support structures [21]. Additionally, wide dispersion on measured backside irradiance has been observed to depend on both the sensor [22] and module position (within an array of modules) [23,24]. The reported non-uniformity, as defined by IEC 60904-1-2 [1], can be as high as 35% in outdoor conditions [24]. Even though the presence of non-uniform back illumination should rarely produce hotspot issues in bPV modules [22], there is at least

one reported case of a considerable increase in local temperatures (+30 °C) caused by the torque tube of an horizontal single-axis tracker (HSAT) [25]. This last fact highlights the importance of paying special attention to the role of mounting structures when dealing with bPV installations.

In order to investigate bifacial performance in the complex scenario of industrial-like rooftops, different tests were carried out. They include a comparison of a bifacial module with two different conventional PV devices (oriented at the optimal monofacial tilt, 30°) and a comparison of two bPV modules with slightly different backlight obstructions.

Accurate simulation tools for bPV modules, which can evaluate their power generation potential under different environmental conditions, are essential for predicting the energy yield of bPV-based solar generators and optimizing their performance [26]. In terms of the electrical model, it is common practice to adapt conventional models for bPV applications. One approach is to incorporate a current source into PV-equivalent circuits to account for photogenerated currents from backside irradiance, resulting in four-, five-, or six-parameter models [27]. Another proposal is to use two conventional models in parallel, one for each surface [28,29]. To fully represent the multiphysics behavior of bPV modules, it is necessary to integrate the electrical model with thermal and optical considerations [30]. Experimental data, like those presented in this study, are critical to evaluate and validate these models or develop new ones.

The sections of this study are as follows: Section 2 describes the experimental setup, the tests, and the methods that allowed us to obtain the results. Section 3 presents and discusses the performance comparison of a bPV module against two different conventional devices and against itself (with an estimated monofacial performance) and, finally, the influence of the mounting structure on the power performance. The last section presents the conclusions of this article.

2. Materials and Methods

2.1. Experimental Setup

All tests were carried out at the SolarTech^{LAB} of the Politecnico di Milano (45.503 N, 9.1566 E). Milan is located in a region with humid subtropical climates, or Cfa, according to the Köppen climate classification. This type of climate is characterized by long hot and humid summers and foggy winters. The test facility is equipped with a meteorological station that records ambient temperatures and humidity, wind speed/direction, global horizontal irradiance (GHI), diffuse horizontal irradiance (DHI), and global tilted irradiance (GTI) at 30°. In the test facility, three PV modules were set up under the same conditions (tilt 30° and azimuth 6.5 E, being 0° south), with a GCH of 17 cm. Two of the modules were conventional monofacial PV devices (henceforth referred to as PV1 and PV2) and the third one of bifacial technology (bPV). In the ground floor surrounding bPV, a high reflecting aluminum foil was placed to increase the incident irradiation on the secondary face of bPV. Aluminum foil albedo is in the range of 0.71–0.78 and has low dependence on solar elevation [31]. The experimental setup is shown in Figure 1.

Module PV1 was manufactured by sunpower with a peak power of 327 W (under standard test conditions, STC: 1000 W/m^2; AM 1.5 spectrum; and module temperature of 25 °C) [32]; PV2 was produced by Aleo and is able to generate up to 305 under identical conditions [33], whereas bPV (a 345-Watt module, with glass/glass frameless structure) was fabricated by 3SUN, and its reported bifaciality (φ) is over 85% [34]. The main characteristics of the modules (PV1, PV2, and bPV) are summarized in Table 1. Apart from some construction features and nominal operating cell temperature (NOCT), it includes a short-circuit current (I_{sc}), open-circuit voltage (V_{oc}), and maximum power (P_{mp} and its components I_{mp} and V_{mp}), as well as the thermal coefficients of I_{sc}, V_{oc}, and P_{mp} (α, β, and γ, respectively).

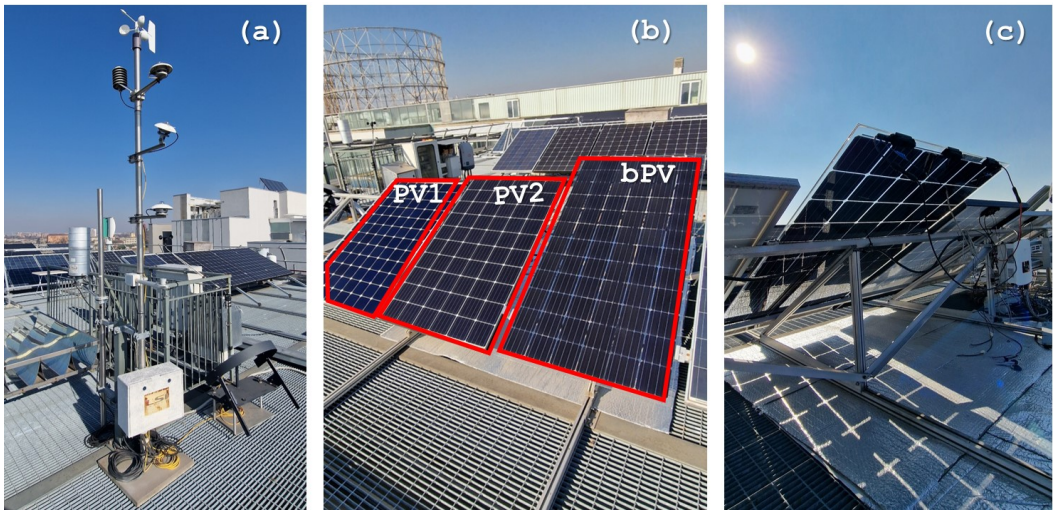

Figure 1. Experimental setup at SolarTech^{LAB} (45.503 N, 9.1566 E). Meteorological station (**a**), PV modules under test (**b**), and back of bPV with high-reflecting ground surface (**c**).

Table 1. Main PV module characteristics.

Manufacturer	**Sunpower**	**Aleo**	**3SUN**
Model	**SPR E20 327 COM**	**S59 305**	**3S Dual 72N**
Short Name	**PV1**	**PV2**	**bPV**
		Mechanical	
Length × width [mm]	1558 × 1046	1660 × 990	1983 × 998
Cell material	m-Si	m-Si	m-Si
Cell size [mm]	125 × 125	156.75 × 156.75	156.75 × 156.75
Number of cells (N_c)	96	60	72 *
		Electric	
P_{mp} [W]	327 (+5/−3 W)	305 (±5 W)	345 (+3%)
V_{mp} [V]	54.7	31.4	39.3
I_{mp} [A]	5.98	9.72	8.78
V_{oc} [V]	64.9	39.6	47.9
I_{sc} [A]	6.46	10.06	9.18
β [mV/°C]	−176.6	−114.84	−143.7
(%/°C)	(−0.272)	(−0.29)	(−0.30)
α [mA/°C]	2.6	5.03	4.4
(%/°C)	(+0.04)	(+0.05)	(+0.048)
γ [%/°C]	−0.35	−0.4	−0.38
NOCT [°C]	45 ± 2	48 ± 2	44 ± 2

* Per face.

During a 5-day campaign, the *I-V* curves of the 3 modules were traced in central day hours. For each condition, 5 curves were obtained per device using an *I-V* tracer manufactured by TeamWare (the process to obtain the five curves takes up to 1.5 min). Additionally, the temperature of each module was measured using type K thermocouples and recorded with a data logger Elo3305, manufactured by LSI. The main characteristics of the equipment used are summarized in Table 2.

Table 2. Technical characteristics of measurement devices at SolarTech^{LAB}.

Equipment	Manufacturer-Model	Other
I-V Tracer	TeamWare-Wally	Voltage, current precision: ±0.5% (2–120% full scale range)
Thermocouple modules	RTD PT100 A Class	Accuracy: 0.25 °C; Resolution: 0.1 °C
Data Logger	LSI-Elo3305	Acquisition rate: 1 Hz
Thermocouple humidity sensor	LSI-DMA875	Pt100 1/3 B (DIN EN 60751); Measurements range: [−30 °C, +70 °C]; Resolution: 0.04 °C; Uncertainty: 0.2 °C (at 0 °C)
Pyranometer (GHI and GTI)	LSI-DPA252	ISO9060 Secondary standard; Spectral range: 285–3000 nm; Response time: 4.5 s; Directional response <±10 W/m^2
Pyranometer (DHI)	LSI-DPA154	ISO9060 First Class; Spectral range: 285–3000 nm; Response time: 16 s; Directional response: <±20 W/m^2

The post-process of the curves consisted of 3 steps:

1. Each set of five curves was translated to the mean irradiance of the event, assuming a constant temperature, as in Procedure 4 of Standard IEC 60891: 2021 [35], shown in Equations (1)–(4):

$$I_1' = I_1 + I_{sc,1}\left(\frac{G_2}{G_1} - 1\right), \quad (1)$$

$$V_1' = V_1 - R_s(I_1' - I_1), \quad (2)$$

$$I_2 = I_1' + \alpha(T_2 - T_1), \quad (3)$$

$$V_2 = V_1' + \frac{T_2 - T_1}{T_1}(V_1' - N_c \cdot \varepsilon) \quad (4)$$

where subscripts 1 and 2 denote the original and target conditions, respectively. The number of cells connected in series N, and the current temperature coefficient α can be seen in Table 1. The internal series resistance R_s and the constant ε, which is independent of temperature and irradiance, were fitted to obtain maximum power and voltage errors within ±0.5% at STC in all the curves. Their values are 0.45 Ω and 1.2936 V, respectively.

2. The curves were resampled at identical voltage values and then averaged to obtain a single smoother curve.
3. Finally, for the averaged curve, the main characteristic values were obtained: I_{sc}, I_{mp}, V_{oc}, V_{mp}, and P_{mp}. The values of I_{sc} and V_{oc} were obtained by local fittings in the region close to short- and open-circuits. In the case of I_{sc}, linear regression was used for voltage under 10 V. For V_{oc} by second order polynomial fitting in the region of $V > V_{mp}$.

An example of the 5 original *I-V* curves and the final one after post-process can be seen in Figure 2.

To compare the performance of the three modules (PV1, PV2, and bPV) with different sizes and characteristics, the values were normalized by taking into account the technical features provided by the manufacturer (see Table 1). Therefore, this normalization ensures an equitable and scientifically rigorous analysis, which allows a fair comparison between PV modules with different characteristics and rated power, through the adoption of normalized indexes, as recommended by international standards [36]. Moreover, PV technologies with different characteristics were selected to reflect the diversity of options available in the

market and to provide a more comprehensive analysis of their performance under various conditions. This research aimed to highlight the practical implications and real-world performance differences that users might encounter, with the reported experimental data.

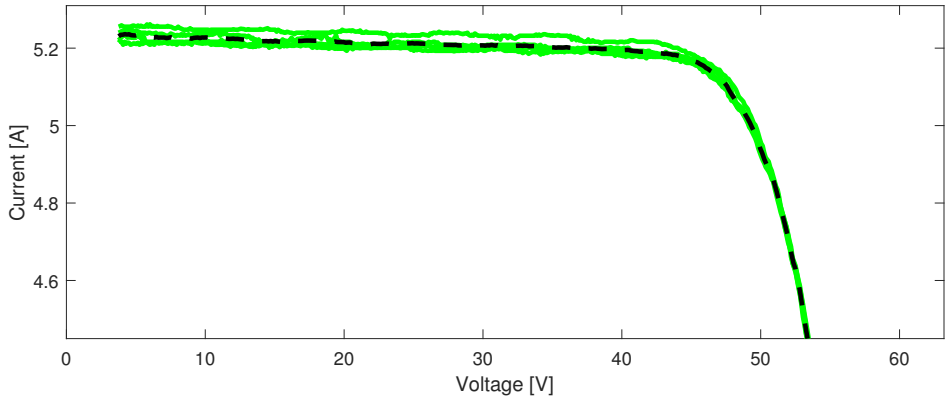

Figure 2. Five original I-V curves (green) and averaged curve (dashed black).

As a final step, the bifacial contribution of bPV was found by subtracting the estimated monofacial P_{mp} from the experimental value. The monofacial power was computed using two independent methods. The first one was carried out by applying Equation (5) [37] as follows:

$$P_{mp}(G,T) = P_{mp,STC} \cdot \frac{G}{G_{STC}}(1 + \gamma(T - T_{STC})) \tag{5}$$

which can be used with the information provided in the manufacturer's datasheet (see Table 1) and experimental or simulated G-T sets.

Additionally, an alternative estimation method was used. It consisted of applying G-T corrections to an experimental *I-V* curve, following Procedure 4 of IEC 60891 [35] (1)–(4), and then finding the maximum power point (MPP). The curve used for the task was obtained by selecting the best sample over a set of different curves traced with the secondary face of bPV being covered (see below).

2.2. Outdoor Characterization of the Bifacial Main Face

The principal face of bPV was tested independently in an earlier experimental campaign. The bPV module was mounted in a tilting structure in "monofacial" configuration (by blocking the secondary face, as can be seen in Figure 3), and the *I-V* curves were traced in a 1-month campaign for different irradiance levels and ambient temperatures.

Then, the curves were processed as described before; all of them were translated to STC conditions, and errors at P_{mp}, V_{oc}, and I_{mp}/I_{sc} were computed. The curve with the lowest sum of absolute estimation errors was selected as follows:

$$err = \left|\frac{P_{mp}}{P_{mp,STC}} - 1\right| + \left|\frac{V_{oc}}{V_{oc,STC}} - 1\right| + \left|\frac{I_{mp}/I_{mp,STC}}{I_{sc}/I_{sc,STC}} - 1\right| \tag{6}$$

In (6), the subscript STC denotes reported values under standard test conditions (see datasheet values in Table 1).

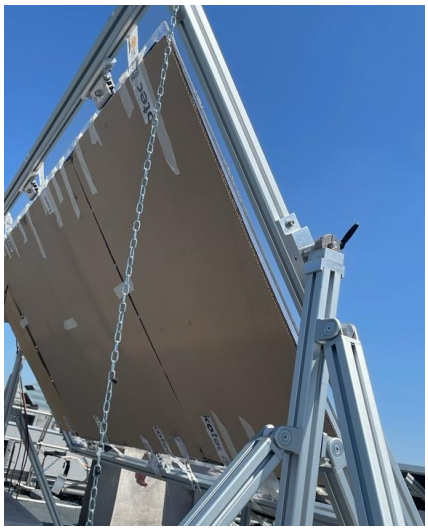

Figure 3. Single-face bPV characterization setup.

2.3. Influence of Mounting Structure

A final test was performed to investigate the influence of the mounting structure on the power output of bifacial modules, specifically the obstruction of back illumination produced by the structure supporting them. In this case, a later-arrived identical pair of bifacial modules (hereinafter referenced as bPV1 and bPV2, model 3S Dual 72N; see Table 1) was mounted side by side with a slight vertical deviation (see Figure 4), which induced each horizontal beam of the structure to partially cover one or two rows of cells (as shown in Figure 4b). In the case of bPV1, the structure partially blocks four rows of PV cells and only the half for bPV2.

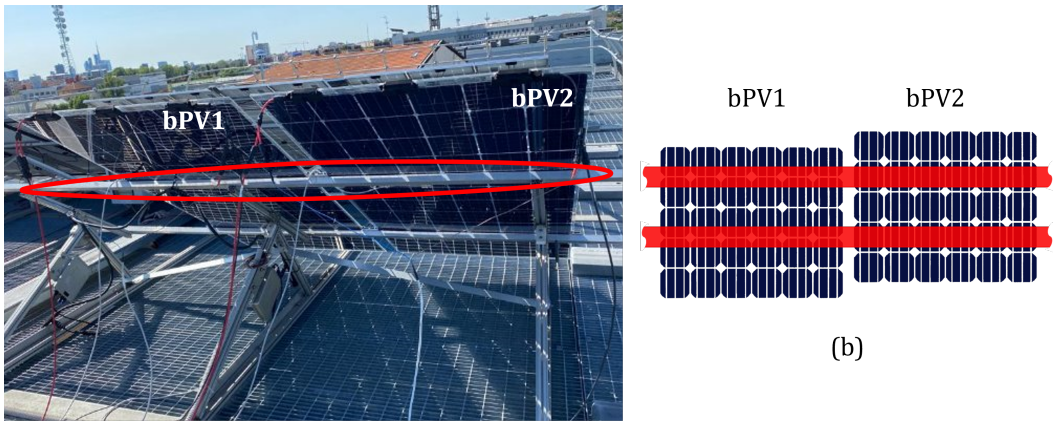

Figure 4. Mounting of bPV1 and bPV2. Experimental setup (**a**) and obstruction scheme (**b**).

As in the previous cases, a set of *I-V* curves of both modules were traced one after the other, which permits the comparison of both of them in almost identical conditions. The set of curves was averaged in the same way as described before.

3. Results and Discussion

3.1. Modules Comparison

For each module, more than 35 sets of *I-V* curves were obtained in an equal number of operation points and as close to each other as possible. Figure 5 shows the in-plane global irradiance, ambient temperature, and time instants required for tracing each set of curves for the three modules. As is observed, the *I-V* curves were obtained in at least one case of

the main sky conditions: three clear-sky days (14–16 February), one with passing clouds (17 February), and a final overcast one (20 February).

A summary of the outdoor results can be seen in Figure 6, where the maximum power (a), short-circuit current (b), open-circuit voltage (c), and modules temperature boxplot (d) can be observed. The superior generation performance of bPV over both PV1 and PV2 is evident (Figure 6a). At three different irradiance levels of 300, 600, and 900 W/m^2, and considering the linear regressions shown on Figure 6a, bPV would proportionally produce up to 6.4% more than PV1 and 7.8% more than PV2 (the remaining values are shown in Table 3).

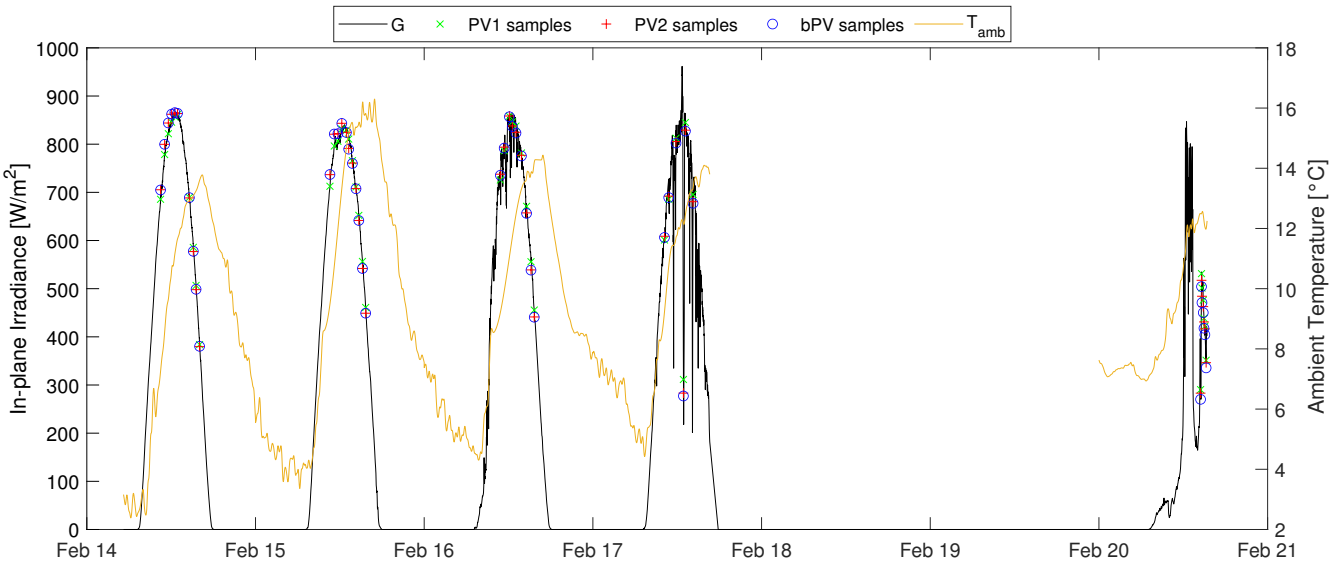

Figure 5. In-plane irradiance (30º), ambient temperature, and instant of *I-V* samples for modules PV1 (green-x), PV2 (red-+), and bPV (blue-o). 18–19 February were not labor days, and no *I-V* curves were obtained.

Table 3. Potential power increment according to linear regressions at different front irradiance levels.

		Front Irradiance 300 W/m^2	600 W/m^2	900 W/m^2
$\frac{P_{mp}}{P_{mp,STC}}$ [%]	PV1	27.5	53.4	79.3
	PV2	26.8	52.3	77.9
	bPV	31.8	58.8	85.7
	bPV-PV1	4.3	5.4	6.4
	bPV-PV2	5.0	6.4	7.8

Similar behaviors can be observed when analyzing the SC current (I_{sc}) (Figure 6b). The bifacial module's current capacity is always higher than the two conventional modules (PV1 presents slightly better characteristics than PV2). Once again, linear fitting allows the quantification of the additional current, the current increments are given at 900 W/m^2: 3.78–5.37% (for PV1 and PV2, respectively).

As expected, no particular OC voltage (V_{oc}) improvement is observed, as bifacial devices modify power through the increase in the total photogenerated current, and this has a logarithmic relationship with V_{oc}. Indeed, bPV demonstrates an intermediate behavior between PV1 and PV2 (Figure 6c).

The temperature operation is a critical performance feature as its increment reduces PV efficiency and accelerates cell degradation [38]. It has been suggested that bifacial modules would operate at lower temperatures than conventional PV ones [39,40], with an estimated reduction of around 1.1 °C [40]. Our experimental results show that it could be the case

but not necessarily (see Figure 6c and Table 4). If bPV and PV1 are compared, a lower temperature is consistently observed in bPV (mean, median, and lowest boxplot values, excluding outliers). However, no significant difference is observed in the same metrics when compared to PV2. More experimental results are required to fully understand these discrepancies. However, from this point of view, it seems that the bifacial modules would operate under temperatures, at most, as conventional PV devices.

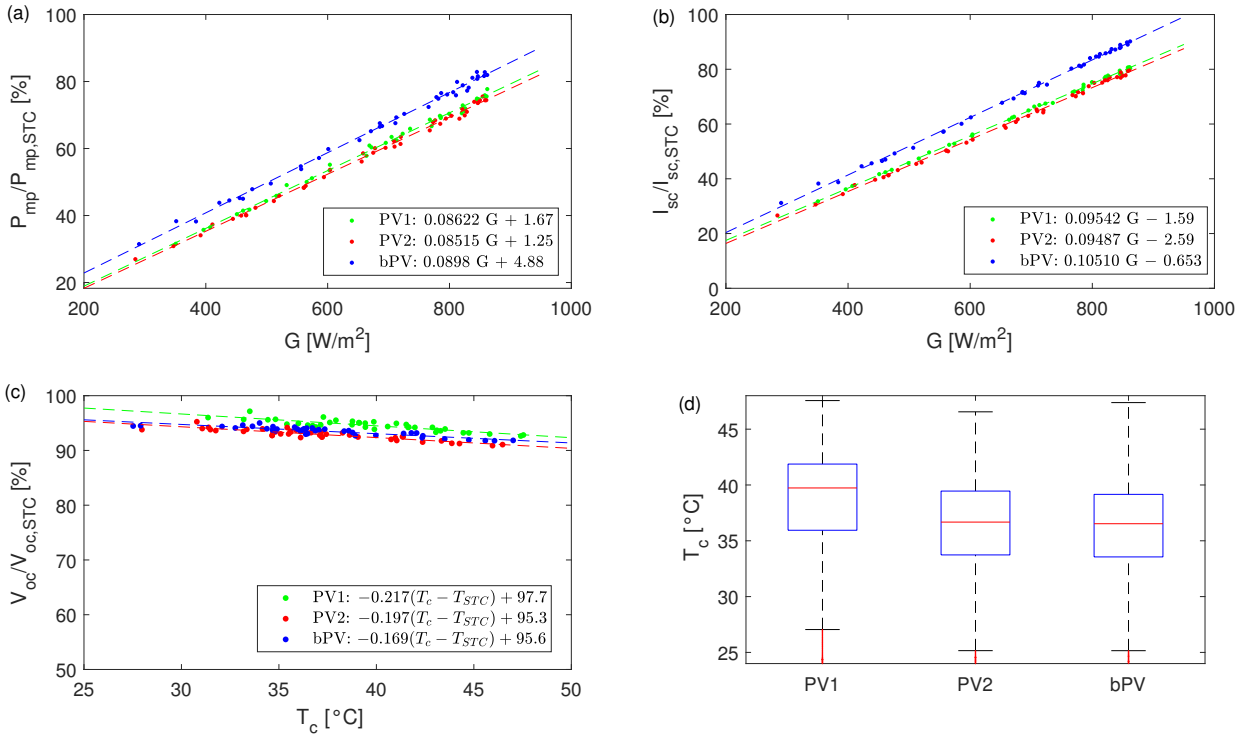

Figure 6. Performance comparison of modules PV1, PV2, and bPV: maximum power (**a**), short−circuit current (**b**), open−circuit voltage (**c**), and cell temperature (**d**). Linear regressions are included in each legend.

Table 4. Some statistical differences in temperature operation.

	PV1	PV2	bPV	PV1-bPV	PV2-bPV
Max [°C]	47.6	46.6	47.4	0.2	−0.8
Median [°C]	39.7	36.7	36.5	3.2	0.2
Mean [°C]	36.9	34.8	34.9	2.0	−0.1
Normal lowest * [°C]	27.0	25.2	25.1	1.9	0.1

* Defined as $Q1 - 1.5(Q3 - Q1)$, where $Q1$ and $Q3$ are the first and third quartile, respectively.

3.2. Bifacial Comparison (Module bPV): Mono vs. Bifacial Performance

In comparison to other PV modules (PV1 and PV2), the bPV module exhibits a superior power capacity, achieving up to a +7.8% increase under the test conditions being analyzed (refer to Figure 6a and Table 3). It is imperative to discern whether this enhancement arises primarily from the secondary PV face or if variances among manufacturers contribute to a fraction of it. This comparison essentially evaluates bPV against itself, considering both mono- and bifacial configurations.

I-V curves' maximum power points of bPV (in monofacial operation) were derived utilizing two distinct methods outlined in the preceding section. Initially, employing Equations (1)–(4), the baseline curve was adjusted to encompass all bPV G-T tracing conditions (as shown in Figure 5), and the MPP was then identified. The second method was then applied using (5) under identical conditions.

Both the measured and estimated maximum power outputs of bPV are depicted in Figure 7, as well as the disparity between the two methods. Both approaches yielded comparable (Figure 7a) and consistent (Figure 7b) outcomes. During days characterized by clear-sky conditions and minimal cloud cover, the additional power output ranged from 1 W to 7 W. However, it notably increased on overcast days (see Figure 5), reaching values within the range of 7 W to 15 W. This observed phenomenon is attributed to a significant reduction in back-side irradiance non-uniformity under high diffuse fraction conditions [10], consequently diminishing the current mismatch on the secondary face and augmenting its power output.

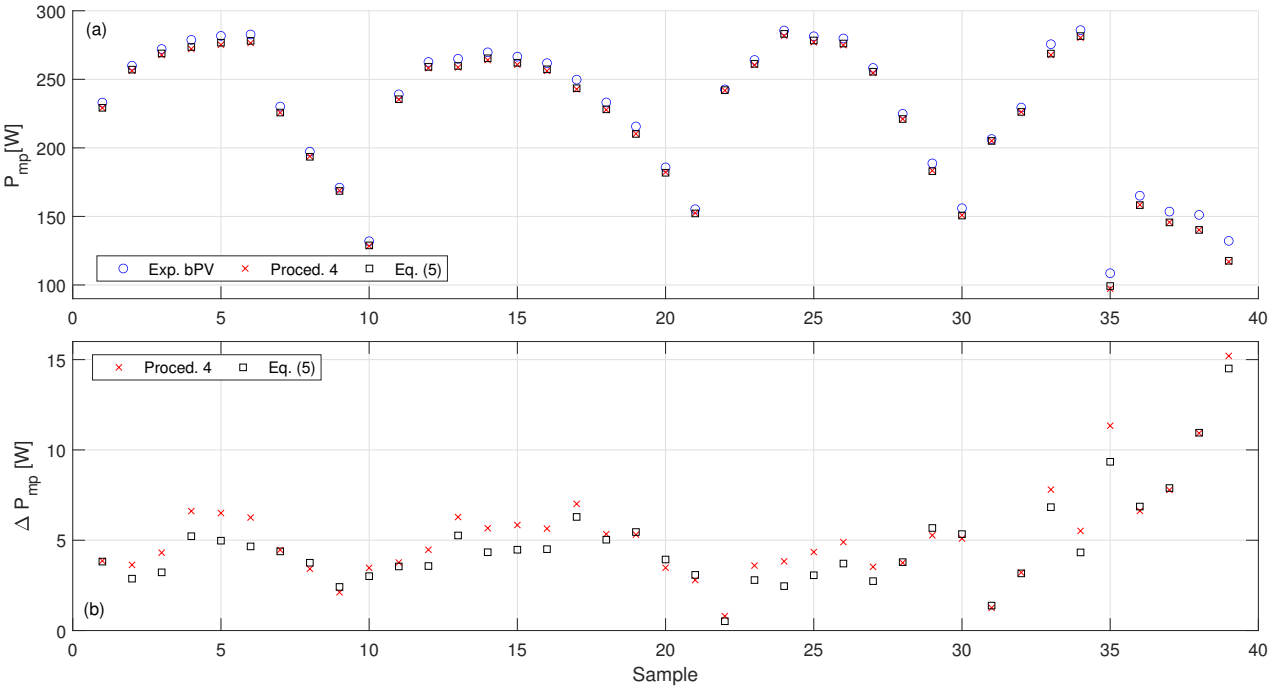

Figure 7. Bifacial–monofacial MPP comparison of bPV module. Recorded MPP of bPV and estimated monofacial by two different methods (**a**) and estimated bifacial contribution (**b**). Estimation methods: Procedure 4 of IEC 60891 [35] (red crosses) and (5) (black squares).

The bifacial power gain (BPG) can be defined (7) to quantify bifacial contribution:

$$BPG = \frac{P_{mp,b}}{P_{mp,m}} - 1 \tag{7}$$

where the b and m subscripts distinguish between bi- and monofacial maximum power, respectively.

When BPG is calculated (7), for clear or marginally covered days, its value is close to 2% (means of 1.7% and 1.9%, depending on the monofacial estimation method, see Figure 8a) but can reach 4%. However, in overcast scenarios, it can be as high as 15%, even under non-favorable test conditions. This is clearly evidenced if BPG is plotted against diffuse fraction (see Figure 8b), where the two clusters are observed. In Figure 8b, the diffuse fraction was calculated on the horizontal plant, that is, directly from measured data (DHI/GHI).

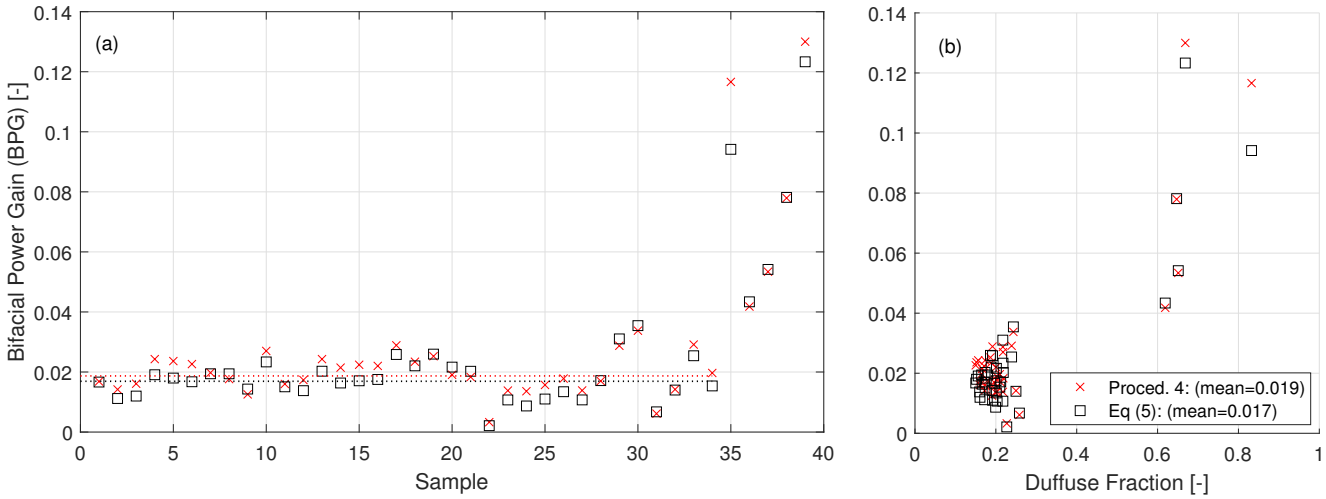

Figure 8. Bifacial power gain of bPV by two P_{mp} estimation methods: Procedure 4 of IEC 60891 [35] (red crosses) and Equation (5) (black squares). Chronological samples (**a**) versus diffuse fraction ratio (**b**). BPG mean of low diffuse fraction samples is added to the legend.

3.3. Influence on Mounting Structure

An additionalfactor contributing to non-uniform rear illumination, in addition to the diffuse fraction, is the structural configuration of the mounting system itself. To elucidate its impact, bPV modules (bPV1 and bPV2) were positioned adjacently with varying frame obstruction patterns, as illustrated in Figure 4. Distinct *I-V* curves were then generated by altering the tilt angle (and in-plane irradiance). In this case, the ground behind bPV modules was a metallic grid (see Figure 4a), and its albedo was found to be 0.09.

Figure 9a presents a representative instance of bifacial devices exhibiting current mismatch on the rear side, attributed to non-uniform illumination, a phenomenon previously observed even under controlled indoor test conditions [41]. Notably, even minor discrepancies in mounting between bPV1 and bPV2 result in discernible deviations in the *I-V* and *P-V* curves. Independently, on the tilt angle, bPV1 shows a worse performance than bPV2, which is more evident at 0º and 30º (see Figure 9b). While bPV1 shows an almost flat *I-V* profile in the range I_{sc}-I_{mp}, three different current levels with two steps (or kinks) are observed in bPV2 in the same range: the first one approximately at 10 V and the second one slightly above 20 V (see Figure 9a).

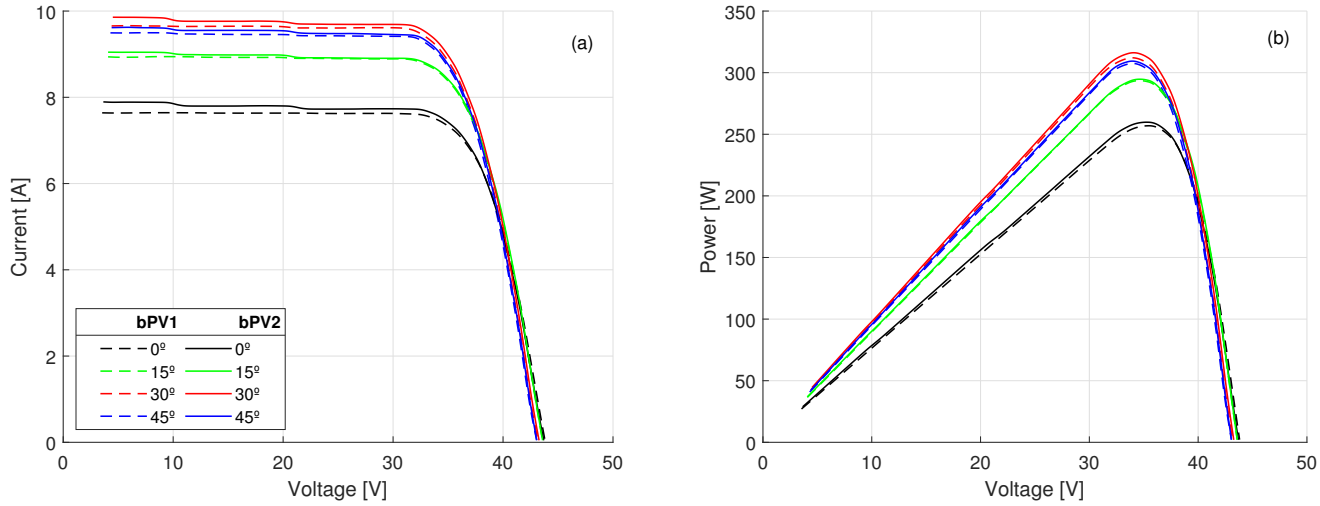

Figure 9. Curves of two identical bifacial modules (bPV1 and bPV2) with different backlight obstruction. *I-V* (**a**) and *P-V* (**b**) curves.

As both bPV1 and bPV2 are bifacial modules of the same model, and their *I-V* curves are traced within a 1.5 min difference, the current discrepancies are only justified by discrepancies in the secondary face contribution. Even if the kinks are more evident in bPV2, their effect is more severe in bPV1, a single deep step, rendering it nearly akin to a conventional device, as the bifacial contribution is largely neglected. Consequently, bPV1 can serve as a reference to estimate the performance reduction in both bPV2 and an ideally placed bifacial module: its current at MPP provides an approximation to that of a conventional device of identical technology; the difference with bPV2 at MPP indicates the additional power/current under the tested conditions; and the discrepancy under the short-circuit conditions facilitates the estimation of the potential current (and power) in the absence of structural obstructions. These approximations are in agreement with the experimental results in similar outdoor setups [21], where an imitated structural beam completely blocks a row of cells in the back face and makes the *I-V* curve coincide with that of a conventional module, i.e., a practical cancellation of the bifacial contribution [21].

Despite the presence of these deviations, which attenuate its bifacial contribution, bPV2 exhibits a slight increase in maximum power across all tested conditions (see Figure 9b and Table 5). The variation in current attributed to the kinks in Figure 10a falls within a similar range (0–3% of I_{sc}), as reported in indoor measurements characterized by non-uniform back radiation [41]. To discern these differences more clearly, the variation (bPV2-bPV1) for all curves is depicted in Figure 10. The values at MPP are denoted by x-markers for bPV1 and o-markers for bPV2. Notably, the changes in voltage at MPP are negligible, indicating that any variation in power is primarily attributable to the changes in current. This can be derived by (8) and (9), where an apostrophe signifies the presence of bifacial contribution (either bPV2 or the ideal scenario of homogeneous illumination without kinks), while its absence denotes the scenario where bifacial contribution is entirely neglected (bPV1).

$$P'_{mp} \approx V_{mp}(I_{mp} + \Delta I'_{mp}) \rightarrow \Delta P'_{mp} = P'_{mp} - P_{mp} \approx V_{mp}\Delta I_{mp} \quad (8)$$

$$\rightarrow \frac{\Delta P'_{mp}}{P_{mp}} = BPG \approx \frac{\Delta I'_{mp}}{I_{mp}} \quad (9)$$

In Equation (9), if the ideal condition is analyzed, $\Delta I'_{mp}$ is approximately $\Delta I'_{sc}$, thereby facilitating the estimation of ideal BPG (refer to Table 5). To derive this estimation, $\Delta I'_{sc}$ was approximated as the median value for voltages below 9 V, considering that the irregularities of the curves preclude confident linear regression analysis for low voltages (before the deepest kink). These medians are depicted as dotted lines for each case in Figure 10a, with the corresponding values provided in Table 5 (ΔI_{sc}).

Table 5. Estimation of BPG for the experimental test and the ideal condition without non-homogeneous illumination.

	bPV2–bPV1		bPV1		BPG			
Tilt [°]	**ΔI_{sc} [A]**	**ΔP_{mp}[W]**	**I_{mp} [A]**	**P_{mp} [W]**	**Ideal [%]**	**bPV2 [%]**	**Δ [%]**	**$\Delta P_{mp,ideal}$ [W]**
0	0.249	2.85	7.25	256.9	3.43	1.11	2.32	8.5
15	0.112	1.16	8.49	293.5	1.32	0.40	0.92	2.7
30	0.196	4.13	9.20	312.1	2.13	1.32	0.81	2.5
45	0.121	1.85	9.06	307.5	1.34	0.60	0.74	2.3

As can be seen in Table 5, the presence of light obstruction by the mounting structure can reduce to a third (tilt 0° or 15°) or half of the potential BPG (tilt 30° or 45°). In addition, as shown in Figure 9, the contribution of the secondary face could be practically wasted.

It is crucial to solve, or at least fully understand, the problem of non-uniform illumination in order to take full advantage of bifacial PVs. Its presence can severely reduce bifacial contribution. This is particularly challenging since low non-uniformity (as the one required in IEC 60904–1–2) is hardly achievable under real outdoor conditions [10] or even in controlled indoor laboratory tests [42].

The impact of non-uniform rear illumination could potentially be reduced by bPV modules of half-cut cells since, in the same sense of partial shading, the current reduction in the secondary face due to non-uniformity would be related to one-sixth, rather than one-third, of the module surface. However, some recent results suggest that half-cut bPV modules could produce a new hotspot phenomenon ("hotspot mirroring") [43]. We are currently conducting tests to investigate in this direction.

An additional mitigation measure has been proposed when reinforced bars are placed in the mounting structure (similar to those in Figure 4) [21]. If the distance between the bars and the module is equal to the beam width, significant BPG recovery (more than 60%) could be achieved by a proper structure configuration (see [21] for more details).

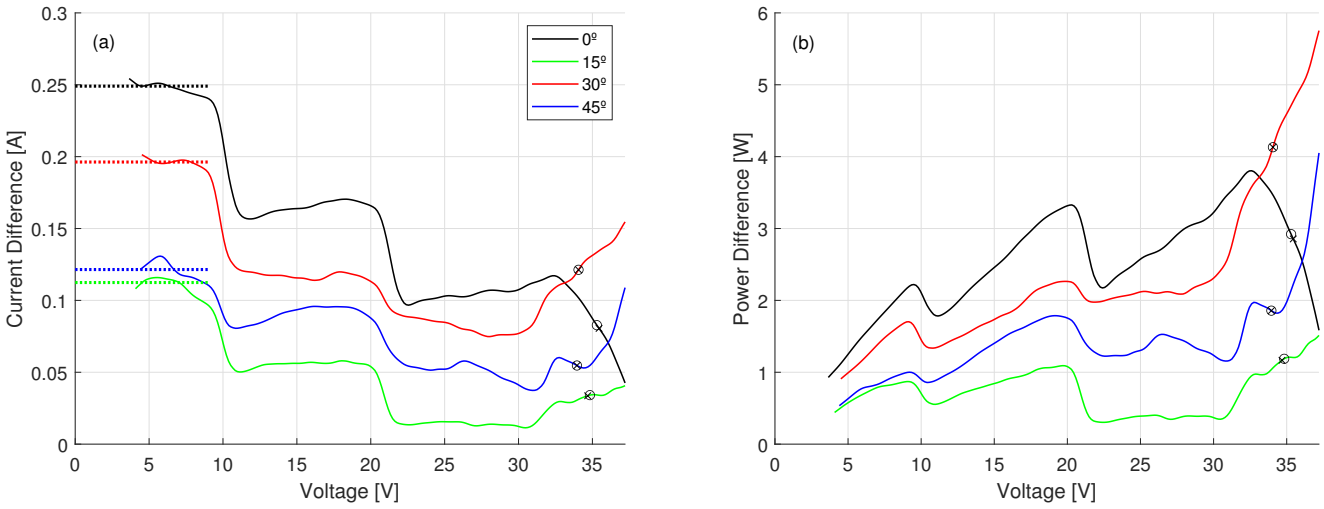

Figure 10. Curves discrepancies (bPV2–bPV1). *I-V* (**a**) and *P-V* (**b**). MPP are identified with × (bPV1) and ○ (bPV2). In (**a**), dotted lines show the estimated current difference at SC.

4. Conclusions

This study investigated the performance of bPV modules in a temperate-climate setting (Cfa, Köppen classification) and an industrial rooftop-like test environment characterized by low ground clearance height (GCH) and limited tilt angles. We elucidated that non-uniform rear-side illumination, stemming from both ambient conditions (e.g., low diffuse to global radiation ratio) and site-specific factors (e.g., mounting structure characteristics), can substantially diminish bifacial performance in these non-ideal operational conditions. Despite the challenges posed by non-uniform rear-side illumination, bPV modules demonstrated considerable advantages over their conventional PV counterparts. Comparative analyses against two different PV modules revealed a consistent power increase of 4.3–7.8% with bPV glass/glass frameless technology. Similarly, a self-comparison of bPV modules in the monofacial configuration, where the rear side was fully obstructed, indicated a bifacial additional power estimate of approximately 2% under clear-sky conditions, which could escalate to 15% in overcast scenarios characterized by a high-diffuse-to-global-radiation ratio.

This study delved into the influence of the mounting structure on bPV module performance across various tilt angles (0°–45°). It was demonstrated that even minor discrepancies in module alignment with structural beams can effectively negate any bifacial contribution. The absence of structural obstruction on clear days yielded an estimated additional power generation of up to 3.43% (+8.8 W), while less pronounced non-uniformity induced by the mounting structure still contributed to power enhancements of 1.3% (+4.13 W).

In essence, these findings underscore the complex interplay between environmental, site-specific, and technological factors in determining the performance of bifacial PV modules. Despite the challenges posed by non-uniform rear-side illumination and mounting structure influence, bPV technology offers performance advantages over conventional PV

modules even in not optimized installations. Further research and technological advancements are warranted to address these challenges and fully unlock the potential of bifacial PV technology in sustainable energy generation applications.

Possible measures to reduce the production losses due to the effect of non-uniform rear-side illumination on industrial-like rooftops could include the use of half-cut cell modules and the proper separation of unavoidable blocking structural components, as well as the careful alignment of structural beams and rear cells. Their combination and alternative solutions still need to be investigated and optimized.

Author Contributions: conceptualization, A.G.-M., D.M. and E.O.; methodology, D.M. and E.O.; software, A.D.; validation, D.M., A.D. and E.O.; formal analysis, A.G.-M.; investigation, A.G.-M. and D.M.; data curation, D.M., A.D. and E.O.; writing—original draft preparation, A.G.-M. and D.M.; writing—review and editing, E.O. and S.L.; visualization, A.G.-M.; supervision, S.L.; project administration, S.L.; funding acquisition, S.L. All authors have read and agreed to the published version of the manuscript.

Funding: This study was conducted within the Agritech National Research Center and received funding from the European Union Next-GenerationEU (PIANO NAZIONALE DI RIPRESA E RESILIENZA (PNRR)—MISSIONE 4 COMPONENTE 2, INVESTIMENTO 1.4—D.D. 1032 17/06/2022, CN00000022) and was also partly carried out within the MOST—Sustainable Mobility Center and received funding from the European Union Next-GenerationEU (PIANO NAZIONALE DI RIPRESA E RESILIENZA (PNRR)—MISSIONE 4 COMPONENTE 2, INVESTIMENTO 1.4—D.D. 1033 17/06/2022, CN00000023).

Institutional Review Board Statement: Not applicable.

Informed Consent Statement: Not applicable.

Data Availability Statement: Data available upon request.

Acknowledgments: The authors would like to thank Gregorio Chiarenza and Riccardo Simonetti for their valuable contributions.

Conflicts of Interest: The authors declare no conflicts of interest.

Abbreviations

The following abbreviations are used in this manuscript:

PV	Photovolatic
BPG	Bifacial Power Gain
bPV	Bifacial Photovoltaic
DHI	Diffuse Horizontal Irradiance
GHI	Global Horizontal Irradiance
GTI	Global Tilt Irradiance
OC	Open-circuit
SC	Short-circuit
MP	Maximum Power
MPP	Maximum Power Point
GCH	Ground Clearance Height
STC	Standard Test Conditions
NOCT	Nominal Operating Cell Temperature
AM	Air Mass
IEC	International Electrotechnical Commission
φ	Bifaciality
G	Irradiance
T	Temperature
N_c	Number of cells
R_s	Series Resistance
I, V	Current, Voltage

I', V'	Intermediate values for IEC 60891 4th method [35]
α	Thermal coefficients of I_{sc}
β	Thermal coefficients of V_{oc}
γ	Thermal coefficients of P_{mp}
Δ	Difference

References

1. *IEC 60904-1-2*; Measurement of Current-Voltage Characteristics of Bifacial Photovoltaic (PV) Devices. International Electrotechnical Commission: Geneva, Switzerland, 2019.
2. Stein, J.; Reise, C.; Castro, J.; Friesen, G.; Maugeri, G.; Urrejola, E.; Ranta, S. *Bifacial Photovoltaic Modules and Systems: Experience and Results from International Research and Pilot Applications. Task 13 Performance, Operation and Reliability of Photovoltaic Systems*; Report IEA-PVPS T13-14:2021; 2021. [CrossRef]
3. Stein, J.S.; Riley, D.; Lave, M.; Hansen, C.; Deline, C.; Toor, F. Outdoor field performance from bifacial photovoltaic modules and systems. In Proceedings of the 2017 IEEE 44th Photovoltaic Specialist Conference (PVSC), Washington, DC, USA, 25–30 June 2017; pp. 3184–3189. [CrossRef]
4. Riedel-Lyngskær, N.; Berrian, D.; Alvarez Mira, D.; Aguilar Protti, A.; Poulsen, P.B.; Libal, J.; Vedde, J. Validation of bifacial photovoltaic simulation software against monitoring data from large-scale single-axis trackers and fixed tilt systems in Denmark. *Appl. Sci.* **2020**, *10*, 8487. [CrossRef]
5. Ogliari, E.; Dolara, A.; Mazzeo, D.; Manzolini, G.; Leva, S. Bifacial and Monofacial PV Systems Performance Assessment Based on IEC 61724-1 Standard. *IEEE J. Photovoltaics* **2023**, *13*, 756–763. [CrossRef]
6. Sun, X.; Khan, M.R.; Deline, C.; Alam, M.A. Optimization and performance of bifacial solar modules: A global perspective. *Appl. Energy* **2018**, *212*, 1601–1610. [CrossRef]
7. Riaz, M.H.; Imran, H.; Younas, R.; Butt, N.Z. The optimization of vertical bifacial photovoltaic farms for efficient agrivoltaic systems. *Sol. Energy* **2021**, *230*, 1004–1012. [CrossRef]
8. Katsikogiannis, O.A.; Ziar, H.; Isabella, O. Integration of bifacial photovoltaics in agrivoltaic systems: A synergistic design approach. *Appl. Energy* **2022**, *309*, 118475. [CrossRef]
9. Abojela, Z.R.K.; Desa, M.K.M.; Sabry, A.H. Current prospects of building-integrated solar PV systems and the application of bifacial PVs. *Front. Energy Res.* **2023**, *11*, 1164494. [CrossRef]
10. Ozkalay, E.; Lopez-Garcia, J.; Pinero-Prieto, L.; Gracia-Amillo, A.; Kenny, R.P. Evaluation of the non-uniformity of rear-side irradiance in outdoor mounted bifacial silicon PV modules. *AIP Conf. Proc.* **2019**, *2147*, 020011. [CrossRef]
11. Riedel-Lyngskær, N.; Ribaconka, M.; Pó, M.; Thorseth, A.; Thorsteinsson, S.; Dam-Hansen, C.; Jakobsen, M.L. The effect of spectral albedo in bifacial photovoltaic performance. *Sol. Energy* **2022**, *231*, 921–935. [CrossRef]
12. Russell, T.C.; Saive, R.; Augusto, A.; Bowden, S.G.; Atwater, H.A. The influence of spectral albedo on bifacial solar cells: A theoretical and experimental study. *IEEE J. Photovoltaics* **2017**, *7*, 1611–1618. [CrossRef]
13. Molin, E.; Stridh, B.; Molin, A.; Wäckelgård, E. Experimental yield study of bifacial PV modules in nordic conditions. *IEEE J. Photovoltaics* **2018**, *8*, 1457–1463. [CrossRef]
14. Yusufoglu, U.A.; Pletzer, T.M.; Koduvelikulathu, L.J.; Comparotto, C.; Kopecek, R.; Kurz, H. Analysis of the annual performance of bifacial modules and optimization methods. *IEEE J. Photovoltaics* **2014**, *5*, 320–328. [CrossRef]
15. Alam, M.; Gul, M.S.; Muneer, T. Self-shadow analysis of bifacial solar photovoltaic and its implication on view factor computation. In Proceedings of the 2021 IEEE Green Energy and Smart Systems Conference (IGESSC), Long Beach, CA, USA, 1–2 November 2021; pp. 1–5. [CrossRef]
16. Krenzinger, A.; Lorenzo, E. Estimation of radiation incident on bifacial albedo-collecting panels. *Int. J. Sol. Energy* **1986**, *4*, 297–319. [CrossRef]
17. Cooke, M. Optimizing Plant Performance with Smart Solar Trackers & Bifacial Technology. In Proceedings of the bifiPV2020 Bifacial Workshop: A Technology Overview, Virtual, 27–28 July 2020.
18. Berrian, D.; Linder, J. Enhanced Bifacial Gain with Optimized Mountings in Photovoltaic Systems. *Sol. RRL* **2023**, *7*, 2300474. [CrossRef]
19. Vasilakopoulou, K.; Ulpiani, G.; Khan, A.; Synnefa, A.; Santamouris, M. Cool roofs boost the energy production of photovoltaics: Investigating the impact of roof albedo on the energy performance of monofacial and bifacial photovoltaic modules. *Sol. Energy* **2023**, *265*, 111948. [CrossRef]
20. Kim, H.; Gao, Y.; Moran, E.; Howle, A.; McSherry, S.; Cira, S.; Lenert, A. High albedo daytime radiative cooling for enhanced bifacial PV performance. *Nanophotonics* **2024**, *13*, 621–627. [CrossRef]
21. Tsuchida, S.; Tsuno, Y.; Sato, D.; Oozeki, T.; Yamada, N. Albedo-Dependent Bifacial Gain Losses in Photovoltaic Modules with Rear-Side Support Structures. *IEEE J. Photovoltaics* **2023**, *13*, 938–944. [CrossRef]
22. Zhang, Y.; Yu, Y.; Meng, F.; Liu, Z. Experimental investigation of the shading and mismatch effects on the performance of bifacial photovoltaic modules. *IEEE J. Photovoltaics* **2019**, *10*, 296–305. [CrossRef]
23. Riedel-Lyngskær, N.; Petit, M.; Berrian, D.; Poulsen, P.B.; Libal, J.; Jakobsen, M.L. A spatial irradiance map measured on the rear side of a utility-scale horizontal single axis tracker with validation using open source tools. In Proceedings of the 2020 47th IEEE Photovoltaic Specialists Conference (PVSC), Calgary, AB, Canada, 15 June–21 August 2020; pp. 1026–1032. [CrossRef]

24. Moreno-Buesa, S.M.; Muñoz-Cerón, E.; Nofuentes Garrido, G.; Gulkowski, S.; de la Casa Higueras, J.; Aguilera Tejero, J. Characterization of bifacial technology Pv systems. *Proc. Inst. Mech. Eng. Part A J. Power Energy* **2024**. [CrossRef]
25. Braga, D.S.; Kazmerski, L.L.; Cassini, D.A.; Camatta, V.; Diniz, A.S.A. Performance of bifacial PV modules under different operating conditions in the State of Minas Gerais, Brazil. *Renew. Energy Environ. Sustain.* **2023**, *8*, 23. [CrossRef]
26. Riaz, M.H.; Imran, H.; Younas, R.; Alam, M.A.; Butt, N.Z. Module technology for agrivoltaics: Vertical bifacial versus tilted monofacial farms. *IEEE J. Photovoltaics* **2021**, *11*, 469–477. [CrossRef]
27. Singh, J.P.; Aberle, A.G.; Walsh, T.M. Electrical characterization method for bifacial photovoltaic modules. *Sol. Energy Mater. Sol. Cells* **2014**, *127*, 136–142. [CrossRef]
28. Bhang, B.G.; Lee, W.; Kim, G.G.; Choi, J.H.; Park, S.Y.; Ahn, H.K. Power performance of bifacial c-Si PV modules with different shading ratios. *IEEE J. Photovoltaics* **2019**, *9.5*, 1413–1420. [CrossRef]
29. Phimu, K.; Singh, K.J.; Dhar, R.S. Novel SPICE Model for bifacial solar cell to increase the renewable power generation. In Proceedings of the 2021 Devices for Integrated Circuit (DevIC), Kalyani, India, 19–20 May 2021; pp. 129–133. [CrossRef]
30. Gu, W.; Ma, T.; Li, M.; Shen, L.; Zhang, Y. A coupled optical-electrical-thermal model of the bifacial photovoltaic module. *Appl. Energy* **2020**, *258*, 114075. [CrossRef]
31. Gul, M.; Kotak, Y.; Muneer, T.; Ivanova, S. Enhancement of albedo for solar energy gain with particular emphasis on overcast skies. *Energies* **2018**, *11*, 2881. [CrossRef]
32. SunPower. SunPower Residential DC Panel Datasheet. SunPower E-Series: E20-327. 2018.
33. Aleo. S59 HE: 300-310 W Datasheet. 2016.
34. Enel Green Power—3 SUN. 3S DUAL 72N Datasheet. 2018.
35. *IEC 60891*; Photovoltaic Devices—Procedures for Temperature and Irradiance Corrections to Measured I–V Characteristics. International Electrotechnical Commission: Geneva, Switzerland, 2021.
36. *IEC 61724-1:2021*; Photovoltaic System Performance—Part 1: Monitoring. International Electrotechnical Commission: Geneva, Switzerland, 2021.
37. Lorenzo, E. *Handbook of Photovoltaic Science and Engineering*; John Wiley: Hoboken, NJ, USA, 2011; chapter Energy collected and delivered by PV modules; pp. 984–1042. [CrossRef]
38. Badran, G.; Dhimish, M. Potential induced degradation in photovoltaic modules: A review of the latest research and developments. *Solar* **2023**, *3*, 322–346. [CrossRef]
39. Lamers, M.; Özkalay, E.; Gali, R.; Janssen, G.; Weeber, A.; Romijn, I.; Van Aken, B. Temperature effects of bifacial modules: Hotter or cooler? *Sol. Energy Mater. Sol. Cells* **2018**, *185*, 192–197. [CrossRef]
40. Liu, T.; Xu, X.; Zhang, Z.; Xiao, J.; Yu, Y.; Jaubert, J.N. Bifacial PV module operating temperature: High or low? A cross-comparison of thermal modeling results with outdoor on-site measurements. In Proceedings of the 2021 IEEE 48th Photovoltaic Specialists Conference (PVSC), Fort Lauderdale, FL, USA, 20–25 June 2021; pp. 2070–2073. [CrossRef]
41. Lopez-Garcia, J.; Casado, A.; Sample, T. Electrical performance of bifacial silicon PV modules under different indoor mounting configurations affecting the rear reflected irradiance. *Sol. Energy* **2019**, *177*, 471–482. [CrossRef]
42. Lopez-Garcia, J.; Menendez, E.G.; Haile, B.; Shaw, D. Characterizing bifacial modules in variable operating conditions. In Proceedings of the 2018 IEEE 7th World Conference on Photovoltaic Energy Conversion (WCPEC) (A Joint Conference of 45th IEEE PVSC, 28th PVSEC & 34th EU PVSEC), Waikoloa, HI, USA, 10–15 June 2018; pp. 1210–1214. [CrossRef]
43. Suarez, S.; Álvarez, J.; Villoslada, D.; Navas, G.; Vilela, J.; Fernandez, I.; Rodríguez-Conde, S. Thermal Issues on Half-Cell Bifacial Modules. A Way Through Albedo and Mismatch Voltage. In Proceedings of the 40th European Photovoltaic Solar Energy Conference and Exhibition, EU PVSEC 2023, Lisbon, Portugal, 18–22 September 2023; pp. 020221-001–020221-003. [CrossRef]